Available online at www.sciencedirect.com
SCIENCE DIRECT
Journal of Colloid and Interface Science 269 (2004) 178–185
JOURNAL OF Colloid and Interface Science
www.elsevier.com/locate/jcis

Effect of interfacial tension on the dynamic behavior of droplet formation during microchannel emulsification

Shinji Sugiura,[a,b,c] Mitsutoshi Nakajima,[a,*] Tatsuya Oda,[d] Mitsuo Satake,[e] and Minoru Seki [f]

[a] *National Food Research Institute, Kannondai 2-1-12, Tsukuba, Ibaraki 305-8642, Japan*
[b] *The Organization for Pharmaceutical Safety and Research, Chiyoda Ku, Tokyo 100-0013, Japan*
[c] *Radiology Division, National Cancer Center Hospital East, Kashiwa, Chiba 277-8577, Japan*
[d] *Department of Surgery, Institute of Clinical Medicine, University of Tsukuba, Tsukuba, Ibaraki 305-8573, Japan*
[e] *Diagnostics Radiology Division, National Cancer Center Hospital, Chuo Ku, Tokyo 104-0045, Japan*
[f] *Department of Chemistry and Biotechnology, The University of Tokyo, Bunkyo-ku, Tokyo 113-8656, Japan*

Received 18 March 2003; accepted 30 July 2003

Abstract

Microchannel (MC) emulsification is a novel technique for producing monodisperse emulsions. In this study, we investigated the effect of interfacial tension on the dynamic behavior of droplet formation with various surfactant concentrations. Interfacial tension did not affect the resultant droplet diameter in lower flow velocity ranges, but it did affect the time-scale parameters. These results were interpreted using the droplet formation mechanism reported in our previous study. At surfactant concentrations below 0.3%, the emulsification behavior was differed from that at higher surfactant concentrations. An analysis of diffusional transfer indicated that dynamic interfacial tension affects the emulsification behavior at lower surfactant concentrations. Dynamic interfacial tension that exceeded the equilibrium value led to a shorter detachment time. This resulted in stable droplet formation of monodispersed emulsions by spontaneous transformation, even at flow velocities above the predicted critical flow velocity. A previous study predicted that the droplet formation would become unstable and polydispersed larger droplets would form over critical flow velocity. Wetting of the MC with the dispersed phase at lower surfactant concentrations induced formation of larger polydispersed droplets at high flow velocities.

Keywords: Microchannel emulsification; Monodispersed emulsion; Droplet formation; Interfacial tension; Dynamic interfacial tension; Surfactant concentration; Sodium dodecyl sulfate; Diffusion; Wetting

1. Introduction

Emulsions have been utilized in various industries, including food, cosmetics, and pharmaceuticals. The stability, rheology, appearance, chemical reactivity, and physical properties of emulsions are influenced by both the average size and the size distribution of the droplets [1–3]. Monodispersed emulsions are useful for fundamental studies since the interpretation of experimental results is much simpler than for polydispersed emulsions [3]. Various instruments have been used to produce emulsions on industrial and laboratory scales, including high-speed blenders, colloid mills, and high-pressure homogenizers [1,4]. The role of surfactants in these emulsification processes is important because they exert dynamic effects on the interface and reduce the interfacial tension. Dynamic interfacial behaviors, such as dynamic interfacial tension, interfacial tension gradients, and interfacial rheological properties (dilational elasticity/viscosity), affect the resulting emulsion [5,6]. The interfacial tension of the droplets is neither constant nor uniform when the droplets are disrupted. The average value of interfacial tension will be greater than at equilibrium if transport of the surfactant between the bulk solution and interface by convective flow and diffusion is slower than both the surface extension of the drops and their break-up. The interfacial tension gradients enable the interface to resist tangential stresses from the adjoining flowing liquid. The Gibbs–Marangoni effect, which is based on interfacial tension gradients, contributes to stabilization against recoalescence. The interfacial viscoelasticity resists movement of the interface.

* Corresponding author.
E-mail address: mnaka@nfri.affrc.go.jp (M. Nakajima).

0021-9797/$ – see front matter
doi:10.1016/j.jcis.2003.07.031

Membrane emulsification is a promising technique for producing emulsions with narrow size distributions [7–9]. The emulsions are produced by pressurizing a dispersed phase into a continuous phase through a microporous membrane; the emulsion droplet size is controlled by the membrane pore size. This technique can be used to prepare emulsions without excessive mechanical stress at a lower energy input than conventional emulsification techniques [10]. The dynamic interfacial tension reportedly affects the emulsification behavior during the membrane emulsification process [10,11].

We recently proposed a novel method for generating monodispersed emulsion droplets from a microfabricated channel array [12]. This emulsification technique is known as microchannel (MC) emulsification. Emulsions with a coefficient of variation of approximately 5% have been successfully prepared by applying this technique. The droplet size is controlled by MC geometry [13,14]. We have applied it to preparations of several types of oil-in-water emulsions, water-in-oil emulsions [15,16], lipid microparticles [17], and polymer microparticles [18]. The role of the surfactant is important in MC emulsification [16,19]. Anionic surfactants and hydrophilic surfactants are suitable for producing oil-in-water emulsions; hydrophobic surfactants are suitable for water-in-oil emulsions. Surfactant molecules maintain a hydrophilic MC surface and prevent wetting of the MC plate with the dispersed phases in production of oil-in-water emulsions [19].

Droplet formation in MC emulsification is based on a unique mechanism. MC emulsification exploits interfacial tension, the dominant force on a micrometer scale, as the driving force for droplet formation [20]. Monodispersed droplets are formed by spontaneous transformation from a distorted (elongated) disklike shape to a spherical shape, driven by interfacial tension. The energy input for MC emulsification is very low compared to the conventional emulsification technique since droplet formation from the MC is based on spontaneous transformation. The droplet diameter can be predicted from the MC structure based on the droplet formation mechanism [14]. The MC structure consists of a narrow channel and a terrace; there is a deeply etched well at the terrace edge. The droplet diameter corresponds to the volume of the dispersed phase flowing into the well during droplet formation, which is determined by terrace length and channel depth. The MC structure also affects the emulsion productivity [21]. Droplet formation behavior changes significantly above the critical flow velocity (U_C). U_C can be predicted by the critical capillary number [21]. Interfacial tension, the driving force of droplet formation in MC emulsification, dominates other forces below U_C. Monodispersed droplets are subsequently formed. The viscous drag force, which induces laminar flow, dominates the interfacial tension above U_C. The dispersed phase consequently flows out continuously like a laminar flow, and larger droplets are formed. The droplet formation behavior is determined by the balance between the interfacial tension and the viscous force.

Considering the droplet formation mechanism in MC emulsification, interfacial tension affects the emulsification behavior. Previous studies investigated the effects of the surfactant on the potential for emulsification and the resultant droplet diameter [15,16,19]. We further investigated the effect of (dynamic) interfacial tension in this study by examining the dynamic droplet formation behavior at different interfacial tensions with various surfactant concentrations.

2. Materials and methods

2.1. Materials

Triolein (purity > 90%) obtained from Nippon Lever B. V. (Tokyo, Japan) was used as the dispersed oil phase, and MilliQ water as the continuous water phase. Sodium dodecyl sulfate (SDS) purchased from Wako Pure Chemical Ind. (Osaka, Japan) was used as the surfactant for emulsification.

2.2. MC emulsification

Figure 1 schematically illustrates the MC plates used in this study, which were described previously [20]. The MC plates were fabricated by photolithography and orientation-dependent etching [23]. The MC structure consists of a channel and a terrace, and there is a deeply etched well over the terrace edge.

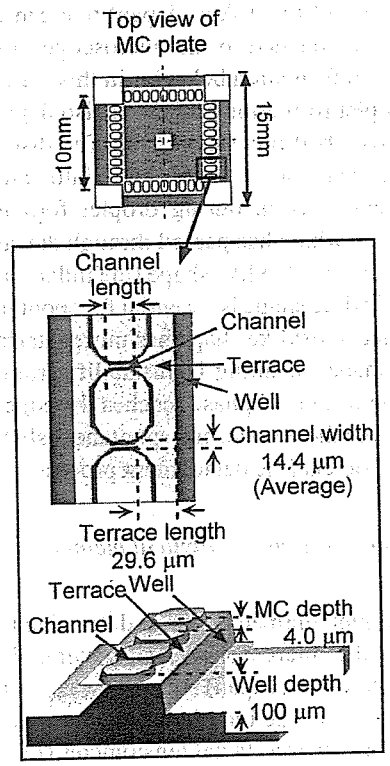

Fig. 1. Schematic of the MC plate.

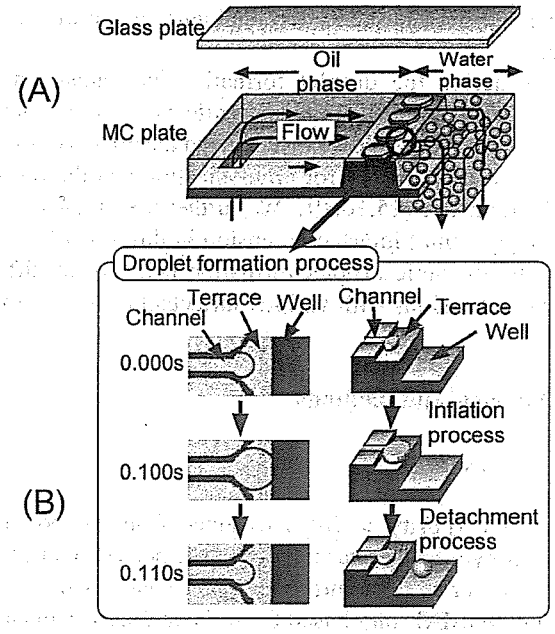

Fig. 2. Schematics of the emulsification process (A) and the droplet formation process (B).

The laboratory-scale apparatus for MC emulsification has been described previously [12]. Figure 2 depicts the schematic flow of the dispersed oil phase through the MC. The emulsification behavior was observed through a glass plate using a microscope video system with a total magnification of ×1000. A high-speed camera (FASTCAM Ultima 1024; Photoron Ltd., Tokyo, Japan) that can capture 16 000 frames/s was attached to the microscope to record the dynamic droplet formation behavior in this study.

The droplet formation process is also depicted in Fig. 2B and was described previously [20]. The distorted dispersed phase is spontaneously transformed into spherical droplets by interfacial tension during droplet formation. The dispersed phase, which has passed through the channel, inflates on the terrace in a disklike shape (the inflation process). This distorted disklike shape is essential for spontaneous transformation since a disklike shape has more interface area than a spherical shape, resulting in instability from interface free energy. The dispersed phase reaches the edge of the terrace, detaches from the terrace, and spontaneously transforms into spherical droplets (the detachment process).

2.3. Measurement and analytical method

The droplet diameters were determined from pictures taken with the microscope video system. Winroof (Mitani Corporation, Fukui, Japan) software was used to analyze the captured images. The interfacial tension was measured with a fully automatic interfacial tensiometer (PD-W; Kyowa Interface Science Co., Ltd., Saitama, Japan) using the pendant drop method.

3. Results and discussion

We first investigated the relationship between the surfactant concentration and the interfacial tension for our experimental system. We used SDS as a surfactant since anionic surfactants are suitable for producing monodispersed emulsions [19]. SDS was dissolved with the water phase. Triolein was used as the oil phase. Figure 3 presents the interfacial tension measurements. We used Fig. 3 to determine the critical micelle concentration (CMC) as 0.28% SDS, which is slightly more than in previous studies [24,25]. This variance from previous studies is reasonable and is attributed to differences in the experimental system and analytical method.

We performed MC emulsification utilizing triolein as the dispersed phase and various concentrations of SDS aqueous solution as the continuous phase. We used surfactant concentrations of 0.05, 0.1, 0.3, and 1.0%. The interfacial tension varied from 3.6 mN/m (1.0% of the surfactant concentration) to 17.5 mN/m (0.05% of the surfactant concentration). We measured the droplet diameter, droplet formation rate, time for inflation, and time for detachment at different flow velocities of the dispersed phase to investigate the dynamic droplet formation behavior. The droplet formation rate is defined as the number of droplets produced within 1 s. We calculated the droplet formation rate in the images captured with the high-speed camera. The inflation time is defined as the time from the endpoint of the previous detachment process (just after the previous droplet formation, 0.00 s in Fig. 2B) to the point at which the dispersed phase reaches the terrace edge (0.10 s in Fig. 2B). The detachment time is defined as the time from the point at which the dispersed phase reaches the terrace edge (0.10 s in Fig. 2B) to the point at which the dispersed phase detaches from the MC and forms separate droplets (0.11 s in Fig. 2B). We measured the inflation time and detachment time in the images captured with the high-speed camera. Details of the time-sequence images were described previously [20]. We examined droplet formation from a single channel located at the center of the terrace line. The flow velocities of the dispersed phase through the channel were calculated from the droplet diameters and

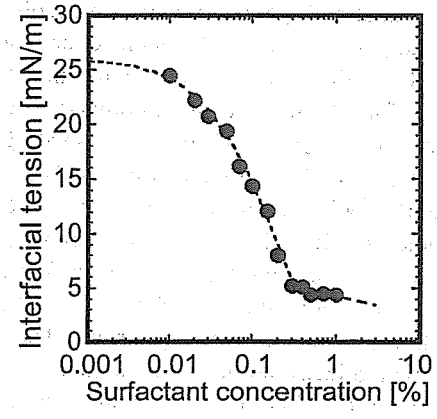

Fig. 3. Relationship between surfactant concentration and interfacial tension.

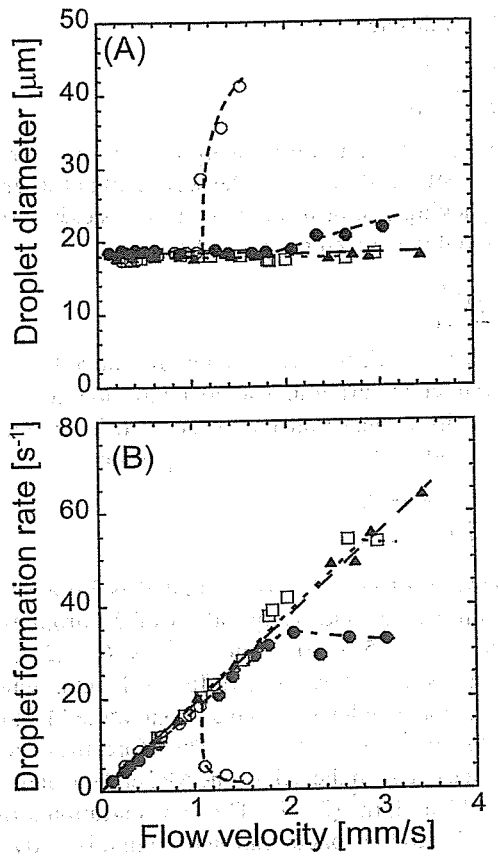

Fig. 4. Effect of interfacial tension on the droplet diameter (A) and droplet formation rate (B) at different flow velocities of the dispersed phase. The SDS concentrations and interfacial tensions were 1.0% and 3.6 mN/m (○), 0.3% and 4.5 mN/m (▲), 0.1% and 13.7 mN/m (□), and 0.05% and 17.5 mN/m (●).

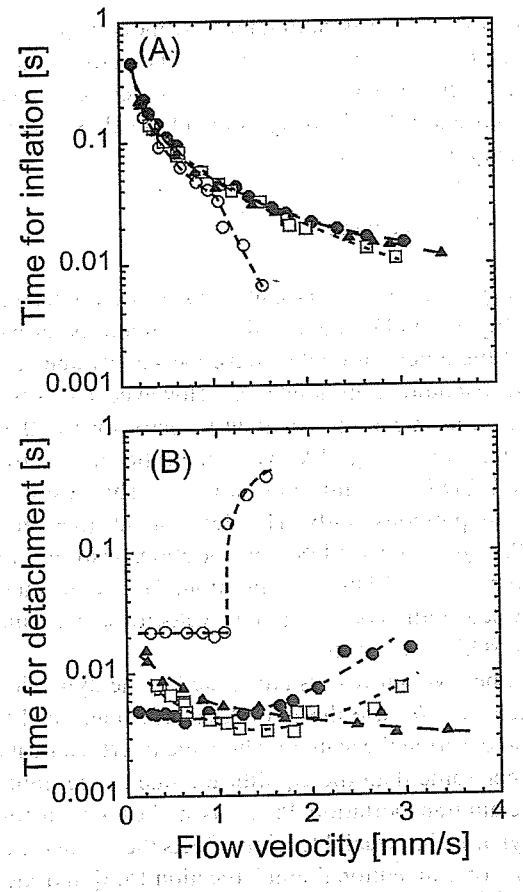

Fig. 5. Effect of interfacial tension on inflation time (A) and detachment time (B) at different flow velocities of the dispersed phase. The SDS concentrations and interfacial tensions were 1.0% and 3.6 mN/m (○), 0.3% and 4.5 mN/m (▲), 0.1% and 13.7 mN/m (□), and 0.05% and 17.5 mN/m (●).

droplet formation rates. MC emulsification was carried out at 25 °C.

Figure 4 illustrates the effect of the interfacial tension on the number-averaged droplet diameters and droplet formation rates at different flow velocities of the dispersed phase. Figure 5 depicts the effect of interfacial tension on inflation time and detachment time at different flow velocities of the dispersed phase. Number-averaged values were used for inflation and detachment times. The experimental results indicated that the formed droplet diameters were independent of the interfacial tension and independent of the flow velocity in lower flow velocity ranges. These results are explained by the droplet formation mechanism described in previous articles [14,20] and depicted in Fig. 2. The previous study demonstrated that the droplet diameter is determined by the volume of the dispersed phase flowing into the well during the detachment process [14]. The results depicted in Fig. 5 indicate that the detachment process is much faster than the inflation process, even though the times for inflation and detachment differed under varied conditions. Therefore, the volume of the dispersed phase flowing into the well can be determined by the MC geometry and is independent of the interfacial tension and flow velocity. Consequently, the interfacial tension and flow velocity did not affect the droplet diameter; they only affected the time-scale parameters for droplet formation.

The inflation times decreased at each SDS concentration in inverse proportion to the flow velocity. This is reasonable since the droplet diameters were independent of the SDS concentration in low flow velocity ranges (Fig. 4A).

The formed droplet diameters were constant below a 1 mm/s flow velocity for a 1% SDS concentration, but increased significantly at velocities over 1 mm/s (Fig. 4A). Other parameters, such as the droplet formation rate and detachment time, also significantly changed at a velocity over 1 mm/s (Figs. 4B and 5). These results are similar to those observed in our previous work [22]. The interfacial tension dominated the other forces at a flow velocity below 1 mm/s (critical flow velocity, U_C), and monodispersed droplets were formed. The viscous force dominated the interfacial tension above U_C. Consequently, the dispersed phase flowed out continuously like a laminar flow, and larger droplets were formed.

The emulsification behavior at 0.3, 0.1, and 0.05% SDS concentrations differed from that at a 1% SDS concentration. The formed droplet diameters were almost constant over a 2 mm/s flow velocity. Spontaneous transformation by in-

terfacial tension was dominant, and monodisperse droplets were formed. Our previous work [22] demonstrated that the critical capillary number (Ca_C), which corresponds to U_C, was constant if the viscosity ratio of both phases and the MC geometry were the same,

$$Ca_C = \frac{\eta U_C}{\gamma} = \text{constant}, \tag{1}$$

where η is the liquid viscosity and γ is the interfacial tension. Equation (1) indicates that U_C should be proportional to γ if the other parameters have the same value, and larger droplets should form above U_C. However, U_C was not observed even at 3 mm/s of flow velocity for the 0.3% SDS concentration in Fig. 4A, while the ratio of γ between 0.3 and 1% SDS concentrations was 1.3. This result conflicts with our previous study. The detachment time profiles for 0.3, 0.1, and 0.05% SDS concentrations also differed from that for the 1% SDS concentration. The detachment times decreased with increasing flow velocities, particularly for lower SDS concentrations.

We believe our results are related to the dynamic interfacial tension. We use the term "dynamic interfacial tension" here to describe the state in which the interfacial tension has a higher value than the equilibrium due to the limitation of surfactant transportation. Previous studies demonstrated that the dynamic interfacial tension affects the emulsification behavior for conventional emulsification [5,6] and membrane emulsification [10]. The dynamic interfacial tension depends on the rate at which the surfactant can be transported to the newly created interface. This transport in the present system is achieved by diffusional transfer since MC emulsification is carried out without a continuous phase flow. The diffusional transfer is composed of two steps. The first step is diffusion in the well from the edge of the MC plate to the terrace (see Fig. 1). The second step is diffusion to the newly created interface in association with the rate of interface extension.

We will first discuss diffusion from the end of the MC plate to the terrace. The diffusional transfer of the surfactant molecule can be estimated from the creation rate of the new interface, assuming that the surfactant molecules immediately adsorb onto the whole newly created interface. New interfaces are created constantly at the exit of the MC during MC emulsification. The interface area (dA/dt) creation rate from one channel is estimated by the equation

$$\frac{dA}{dt} = N\pi d^2, \tag{2}$$

where N is the droplet formation rate and d is the droplet diameter. The surfactant molecules that absorb onto the interface are transferred by diffusion from the end of the MC plate to the exit of the MC (near the terrace line). The surfactant flux (j) necessary for adsorption onto the whole newly created interface is calculated by assuming that the surfactant molecules diffuse in the water phase between the close packed oil droplets,

$$j = \frac{N\pi d^2 \Gamma_\infty}{lh(1-p)}, \tag{3}$$

where Γ_∞ is the saturation adsorption, l is the interval length between MCs (90 μm), h is the well depth (100 μm), and p is the packing rate of hexagonal closed packing (0.74). The diffusion flux is given by Fick's law as

$$j = -D\frac{dC}{dx}, \tag{4}$$

where D is the diffusion coefficient for the SDS and C is the surfactant concentration. The concentration gradient necessary for diffusional transfer in the well is calculated from Eqs. (3) and (4) by the following equation:

$$\frac{dC}{dx} = \frac{-N\pi d^2 \Gamma_\infty}{Dlh(1-p)}. \tag{5}$$

The value of $-dC/dx$ is calculated as 3.6×10^4 mol/m^4 based on Eq. (5) and using values of 20 droplets/s as N, 18 μm as d, 2.5×10^{-6} mol/m^2 as Γ_∞ [25], and 6×10^{-10} m^2/s as D [26]. The diffusion length, which corresponds to the well length from the exit of the MC to the edge of the MC plate, is 3×10^{-4} m. Therefore, the concentration difference between the exit of the MC and the end of the MC plate is 11 mol/m^3 (0.3%). This concentration difference is comparable to the concentration used in this study, although the value of Γ_∞ is different in other articles. It is difficult to reach saturation adsorption at the exit of MC when the surfactant concentration is less than 0.3%. The diffusional transfer rate of the surfactant in the well appears to affect the dynamic interfacial tension, and the dynamic interfacial tension subsequently exceeds the equilibrium value.

We will next discuss the second step, the diffusion rate compared with the interface extension. The effect of diffusional transfer is evaluated by comparing the relative rate of interface extension, $\delta \ln A/\delta t$, with the diffusion time scale, τ_d [6]. The diffusion is too slow at relatively high extension rates to resupply the expanding interface, which will behave as an emulsifier-free interface:

$$\frac{\delta \ln A}{\delta t} \gg (\tau_d)^{-1} \rightarrow \gamma \approx \gamma^0. \tag{6}$$

The emulsifier diffusion is fast enough for the interfacial tension to achieve equilibrium at sufficiently low rates of interface extension:

$$\frac{\delta \ln A}{\delta t} \ll (\tau_d)^{-1} \rightarrow \gamma \approx \gamma^{\text{eq}}. \tag{7}$$

The value of $\delta \ln A/\delta t$ corresponds to the change in interface area during the inflation process. We roughly estimated it using the following equation from the image captured with the high-speed camera,

$$\frac{\delta \ln A}{\delta t} \approx \frac{\ln A_2 - \ln A_1}{\Delta t_i}, \tag{8}$$

where A_1 and A_2 are the interface areas before and after the inflation process (840 and 2240 μm^2) and Δt_i is the time for

the inflation process. The value of $\delta \ln A/\delta t$ is estimated as 20 (s^{-1}) using the value of 0.05 s as the inflation process time. The adsorption kinetics for the ionic surfactant have been studied in depth [23,27,28], although they are not as simple as the nonionic surfactant because of the existence of an electrical double layer. The theoretical model predicts τ_d to be on the order of 10^{-3} to 10^{-4} s for an SDS concentration of 0.03% [27]. Measurements using the capillary-wave method [23] also yield an adsorption relaxation time on the order of 10^{-3} s for SDS in concentration ranges similar to those in our experiment. These values seem rapid compared to the interface extension estimated by Eq. (8), although τ_d is affected significantly by the surfactant concentration, and the actual surfactant concentration at the exit of MC is unknown due to the limitation of diffusional transfer in the well. Therefore, the rate-determining step for diffusional transfer is the first step, i.e., diffusional transfer from the edge of the MC plate in the well.

The above discussion suggests that the dynamic interfacial tension during MC emulsification may exceed the equilibrium value. The dynamic interfacial tension is greater at lower surfactant concentrations and higher flow velocities because the diffusion of SDS molecules is slow and creation of the new interface is accelerated. Greater dynamic interfacial tensions led to shorter detachment times, which accords with the experimental results (Fig. 5). These phenomena were not observed at a 1% SDS concentration because transfer of the SDS molecules is sufficiently high relative to the creation of new interfaces.

The droplet diameters were constant above a 1 mm/s flow velocity for SDS concentrations of less than 0.3%, even though the droplet diameters increased significantly at a velocity over 1 mm/s for the 1% SDS concentration. The increased dynamic interfacial tensions of lower SDS concentrations contribute to the stable droplet formation driven by interfacial tension, even in higher flow velocity ranges. This enables droplets to form by spontaneous transformation at high flow velocities of 2 to 3 mm/s. However, the emulsification behavior depends on the position of the MC. The data shown in Figs. 4 and 5 were measured for MCs at the center of the terrace line. The dispersed phase flowed out at a lower flow velocity for MCs near the end of the terrace than for MCs near the center of the terrace, primarily because the diffusion efficiency depends on the geometry of the MC plate. MCs near the end of the terrace have an advantage in diffusional transfers because no MCs are fabricated at the outer 150 μm of the terrace. Therefore, surfactant molecules diffuse into the newly formed interfaces more easily near the end of the terrace than at the center. The dynamic interfacial tension near the end of the terrace was lower than that at the center, resulting in an outflow of dispersed phase at a lower flow velocity. Comprehensive and quantitative treatment of the dynamic interfacial tension is complicated because it is affected by MC geometry, the position of the terrace line on the MC plate, and diffusion onto the newly created interface. Quantitative treatments for cross-flow MC plates [29] and straight-through MC plates [30] are more complicated because they include convective transfer of the surfactant. However, clarifying the dynamic interfacial behavior is important for designing an MC emulsification process and for understanding the MC emulsification phenomena.

The droplet formation behavior changed for 0.05% SDS concentrations at flow velocities exceeding 2 mm/s. The droplet diameter increased slightly, the droplet formation rate was not proportional to the flow velocity, and the detachment time gradually increased. The same phenomena were observed for a 0.1% SDS concentration at a 2.6 mm/s flow velocity. These phenomena are probably due to the wetting of the MC with the dispersed phase. Figure 6 depicts the detachment process from a wetted channel. The wetted part displayed in the broken circle disturbs the movement of the interface, resulting in the formation of larger droplets. The MC plate must be wetted with a continuous water phase for stable droplet formation [19]. Surfactant molecules adsorbed onto the interface keep the water molecules between

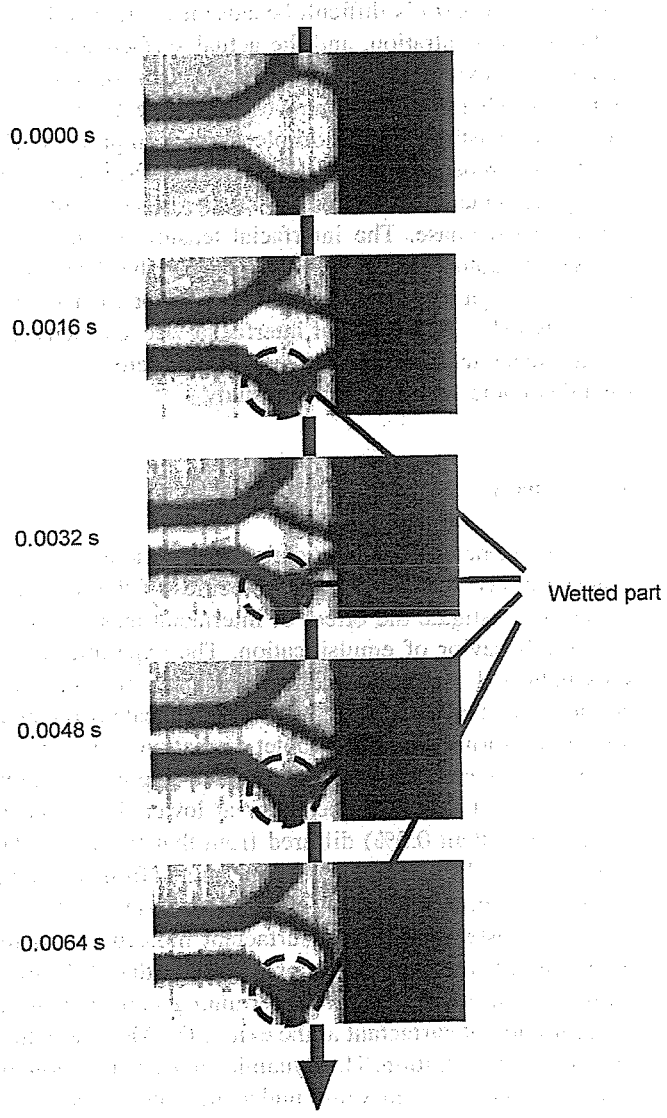

Fig. 6. Detachment from a wetted MC.

the oil–water interface and the MC plate. However, the adsorption layer of SDS molecules on the oil–water interface becomes thinner for lower surfactant concentrations at high flow velocities due to the diffusional transfer limitation, and the dispersed phase wets the MC plate. This leads to larger droplet formation and longer detachment times. The significant limitations of the diffusional transfer caused the MC wetting with the dispersed phase to become conspicuous at higher flow velocities for lower SDS concentrations.

The effect of interfacial viscoelasticity and the interfacial tension gradient cannot be neglected in these flow velocity ranges (2 mm/s for 0.05% SDS concentration, 2.6 mm/s for 0.1% SDS concentration). We use the term "interfacial viscoelasticity" here for the force resisting interface movement. Interfacial viscoelasticity can increase the effective viscosity of the droplet phase by more than an order of magnitude during conventional emulsification under specific conditions [6]. The time scale of the detachment process is close to τ_d, 10^{-3} s, at high flow velocities, although accurate determination of τ_d is difficult because it is affected by the surfactant concentration, and the actual surfactant concentration at the exit of MC depends on the diffusional transfer in the well. Therefore, we cannot deny the effect of the interfacial viscoelasticity on the droplet formation process. The interfacial viscoelasticity may resist the interface movement during the detachment process and could induce outflow of the dispersed phase. The interfacial tension gradient may also resist rupture of the interface during the detachment process through the Marangoni effect, as reported in a previous study [31]. The effects of interfacial viscoelasticity and the interfacial tension gradient may be of interest; however, we did not note any effects in this study.

4. Summary

We performed MC emulsification with various surfactant concentrations at different flow velocities of the dispersed phase to investigate the effect of interfacial tension on the dynamic behavior of emulsification. The experimental results indicated that interfacial tension does not affect the droplet diameter, but affects only the time-scale parameters for droplet formation. The droplet formation behavior at a 1% SDS concentration correlated with our previous study, but the droplet formation behavior at lower SDS concentrations (less than 0.3%) differed from that for a 1% SDS concentration. These results were interpreted from the standpoint of dynamic interfacial tension. Analyses of the diffusional transfer rate of the surfactant molecules and the time-scale of interface extension indicated that diffusional transfer in the well is the rate-determining step and that the concentration of surfactant at the exit of the MC is less than the initial concentration. The dynamic interfacial tension exceeded the equilibrium value under these conditions. This led to short detachment times and droplet formation caused by spontaneous transformation, even at high flow velocities of the dispersed phase. The effect of dynamic interfacial tension was significant, particularly at lower surfactant concentrations and higher flow velocities of the dispersed phase. The droplet formation behavior was also affected by wetting of the MC with the dispersed phase at lower SDS concentrations, inducing formation of larger droplets at high flow velocities. A time-scale analysis indicated that the effect of interfacial viscoelasticity cannot be disregarded. Our results for the effects of dynamic interfacial behavior are useful for designing an MC emulsification process and interpreting the MC emulsification phenomena.

Acknowledgments

This work was supported by the Nanotechnology Project, Ministry of Agriculture, Forestry and Fisheries, and the Program for Promotion of Fundamental Studies in Health Sciences of the Organization for Pharmaceutical Safety and Research of Japan.

References

[1] D.J. McClements, Food Emulsions: Principles, Practice, and Techniques, CRC, Boca Raton, 1999.
[2] E. Dickinson, An Introduction to Food Colloids, Oxford Univ. Press, Oxford, 1992.
[3] T.G. Mason, A.H. Krall, H. Gang, J. Bibette, D.A. Weitz, in: P. Becher (Ed.), Encyclopedia of Emulsion Technology, Vol. 4, Dekker, New York, 1996, p. 299.
[4] P. Walstra, in: P. Becher (Ed.), Encyclopedia of Emulsion Technology, Vol. 1, Dekker, New York, 1983, p. 57.
[5] W.J. Phillips, R.W. Graves, R.W. Flumerfelt, J. Colloid Interface Sci. 76 (1980) 350.
[6] E.H. Lucassen-Reynders, K.A. Kuijpers, Colloids Surf. 65 (1992) 175.
[7] T. Nakashima, M. Shimizu, M. Kukizaki, Key Eng. Mater. 61/62 (1991) 513.
[8] S.M. Joscelyne, G. Trägårdh, J. Membr. Sci. 169 (2000) 107.
[9] A.J. Abrahamse, A. van der Padt, R.M. Boom, W.B.C. de Heij, AIChE J. 47 (2001) 1285.
[10] V. Schröder, O. Behrend, H. Schubert, J. Colloid Interface Sci. 202 (1998) 334.
[11] V. Schröder, H. Schubert, Colloids Surf. A 152 (1999) 103.
[12] T. Kawakatsu, Y. Kikuchi, M. Nakajima, J. Am. Oil Chem. Soc. 74 (1997) 317.
[13] T. Kawakatsu, G. Trägårdh, Y. Kikuchi, M. Nakajima, H. Komori, T. Yonemoto, J. Surfact. Deterg. 3 (2000) 295.
[14] S. Sugiura, M. Nakajima, M. Seki, Langmuir 18 (2002) 3854.
[15] T. Kawakatsu, G. Trägårdh, C. Trägårdh, M. Nakajima, N. Oda, T. Yonemoto, Colloids Surf. A 179 (2001) 29.
[16] S. Sugiura, M. Nakajima, H. Ushijima, K. Yamamoto, M. Seki, J. Chem. Eng. Jpn. 34 (2001) 757.
[17] S. Sugiura, M. Nakajima, J. Tong, H. Nabetani, M. Seki, J. Colloid Interface Sci. 227 (2000) 95.
[18] S. Sugiura, M. Nakajima, H. Itou, M. Seki, Macromol. Rapid Commun. 22 (2001) 773.
[19] J. Tong, M. Nakajima, H. Nabetani, Y. Kikuchi, J. Surfact. Deterg. 3 (2000) 285.
[20] S. Sugiura, M. Nakajima, S. Iwamoto, M. Seki, Langmuir 17 (2001) 5562.
[21] S. Sugiura, M. Nakajima, M. Seki, Langmuir 18 (2002) 5708.

[22] S. Sugiura, M. Nakajima, N. Kumazawa, S. Iwamoto, M. Seki, J. Phys. Chem. B 106 (2002) 9405.
[23] Y. Kikuchi, K. Sato, H. Ohki, T. Kaneko, Microvascular Res. 44 (1992) 226.
[24] M. Sasaki, T. Yasunaga, N. Tatsumoto, Bull. Chem. Soc. Jpn. 50 (1977) 858.
[25] A. Bonfillon, D. Langevin, J. Colloid Interface Sci. 168 (1994) 497.
[26] B. Lindman, M.-C. Puyal, N. Kamenka, R. Rymdén, P. Stilbs, J. Phys. Chem. 88 (1984) 5048.
[27] P.M. Vlahovska, K.D. Danov, A. Mehreteab, G. Broze, J. Colloid Interface Sci. 192 (1997) 194.
[28] V.B. Fainerman, E.H. Lucassen-Reynders, Adv. Colloid Interface Sci. 96 (2002) 295.
[29] T. Kawakatsu, H. Komori, M. Nakajima, Y. Kikuchi, T. Yonemoto, J. Chem. Eng. Jpn. 32 (1999) 241.
[30] I. Kobayashi, M. Nakajima, K. Chun, Y. Kikuchi, H. Fujita, AIChE J. 48 (2002) 1639.
[31] P. Walstra, Chem. Eng. Sci. 48 (1993) 333.

Available online at www.sciencedirect.com
SCIENCE DIRECT
ELSEVIER
Journal of Colloid and Interface Science 270 (2004) 221–228
JOURNAL OF Colloid and Interface Science
www.elsevier.com/locate/jcis

Preparation characteristics of water-in-oil-in-water multiple emulsions using microchannel emulsification

Shinji Sugiura,[a,b,c] Mitsutoshi Nakajima,[a,*] Koji Yamamoto,[a] Satoshi Iwamoto,[a] Tatsuya Oda,[d] Mitsuo Satake,[e] and Minoru Seki[f]

[a] *National Food Research Institute, Kannondai 2-1-12, Tsukuba, Ibaraki 305-8642, Japan*
[b] *The Organization for Pharmaceutical Safety and Research, Chiyoda Ku, Tokyo 100-0013, Japan*
[c] *Radiology Division, National Cancer Center Hospital East, Kashiwa, Chiba 277-8577, Japan*
[d] *Department of Surgery, Institute of Clinical Medicine, University of Tsukuba, Tsukuba, Ibaraki 305-8573, Japan*
[e] *Diagnostics Radiology Division, National Cancer Center Hospital, Chuo Ku, Tokyo 104-0045, Japan*
[f] *Department of Chemistry and Biotechnology, The University of Tokyo, Bunkyo-ku, Tokyo 113-8656, Japan*

Received 18 March 2003; accepted 1 August 2003

Abstract

Microchannel (MC) emulsification is a novel technique for preparing monodispersed emulsions. This study demonstrates preparing water-in-oil-in-water (W/O/W) emulsions using MC emulsification. The W/O/W emulsions were prepared by a two-step emulsification process employing MC emulsification as the second step. We investigated the behavior of internal water droplets penetrating the MCs. Using decane, ethyl oleate, and medium-chain triglyceride (MCT) as oil phases, we observed successful MC emulsification and prepared monodispersed oil droplets that contained small water droplets. MC emulsification was possible using triolein as the oil phase, but polydispersed oil droplets were formed from some of the channels. No leakage of the internal water phase was observed during the MC emulsification process. The internal water droplets penetrated the MC without disruption, even though the internal water droplets were larger than the resulting W/O/W emulsion droplets. The W/O/W emulsion entrapment yield was measured fluorometrically and found to be 91%. The mild action of droplet formation based on spontaneous transformation led to a high entrapment yield during MC emulsification.

Keywords: Microchannel emulsification; Monodispersed emulsion; Droplet formation; Multiple emulsion; Water-in-oil-in-water emulsion; Double emulsion; Entrapment yield; Viscosity

1. Introduction

Multiple emulsions have been studied since 1925, when Seifriz pioneered this work [1]. A water-in-oil-in-water (W/O/W) emulsion consists of internal water droplets dispersed within larger oil droplets, which themselves have been dispersed in an external aqueous continuous phase. As Sherman noted [2], a multiple emulsion is obtained unexpectedly during ordinary emulsification procedures at high concentrations of the dispersed phase or the emulsifying agent, due to either phase inversion [1,3], or to the migration of the emulsifying agent between the two phases of the emulsion [4]. The two-step emulsification method is a reliable method for preparing W/O/W emulsions [5]. The first step in emulsification, providing the ordinary W/O emulsion, was accomplished with a hydrophobic surfactant (low HLB). The second step, providing the W/O/W dispersion, was then carried out by mixing the W/O emulsion within an aqueous solution of hydrophilic surfactant (high HLB).

W/O/W emulsions have primarily been investigated as vehicles for various hydrophilic drugs (vitamins, hormones, and enzymes) that are expected to have prolonged release profiles [6,7]. Multiple emulsions designed as drug delivery systems would be significant in the controlled release of oral, topical, or parenteral administrations when the stability and release mechanisms can be more clearly understood and monitored.

Recently, research has been conducted to create stable multiple emulsions [8–11]. Stability of W/O/W emulsions is generally understood as the resistance of the individual globules to coalescence. The breakdown of a W/O/W emulsion

* Corresponding author.
E-mail address: mnaka@nfri.affrc.go.jp (M. Nakajima).

0021-9797/$ – see front matter
doi:10.1016/j.jcis.2003.08.021

is described through several possible mechanisms [12], including (i) coalescence of the internal aqueous droplets into larger internal droplets; (ii) coalescence of the oil droplets suspended in the external aqueous phase; (iii) expulsion of the internal droplets following rupture of the thin oil films during the interaction of the internal and external aqueous phases; and (iv) swelling or shrinking due to water permeation through the oil membrane by diffusion.

Monodispersed multiple emulsions are useful for both industrial applications and basic studies. Rheology, appearance, chemical reactivity, and physical properties are influenced by both the average size and size distribution, and drug-release properties from multiple emulsions depend on their size. Furthermore, monodispersed emulsions can be very effective in determining the resistance to coalescence of an emulsion due to the ease of observation, and in detecting the water permeation through the oil membrane by diffusion. If the droplet diameter distribution is narrow, the effect of Ostwald ripening is reduced because the effective Laplace pressure is low.

Monodispersed emulsions can be obtained by fractionation from polydispersed emulsion, but repeated operations are required [13,14]. Several research groups are investigating how to produce quasi-monodisperse W/O/W emulsions. Membrane emulsification, in which the pressurized dispersed phase permeates a microporous membrane and forms emulsion droplets, enables us to produce monodispersed emulsions with a coefficient of variation of approximately 10% [15]. This technique has been applied to W/O/W emulsions [16–18]. However, it is not clear how internal water droplets penetrate through the membrane pore. Mason and Bibette proposed that the shear rupturing in couette flow is applicable to producing monodisperse emulsions [19]. This technique has been applied to preparing quasi-monodispersed W/O/W emulsions [20].

Recently, we proposed a novel method for making monodisperse emulsion droplets using a microfabricated channel array [21]. This emulsification technique is called microchannel (MC) emulsification. Oil-in-water emulsions with a coefficient of variation of less than 5% and a droplet size of 3 to 100 μm have been successfully prepared using this technique. The droplet size is controlled by MC geometry [22,23]. An advantage of this technique is direct observation of emulsification through a microscope [21]. We have applied this technique to preparing several types of oil-in-water emulsions, water-in-oil emulsions [25,26], lipid microparticles [27], and polymer microparticles [28]. A disadvantage is its low production rate. Usually, less than 1 ml/h of dispersed phase can be emulsified. A straight-through type MC has been devised to scale this technique up, and the droplet formation volume rate reached 6.5 ml/h of dispersed phase per MC plate [24]. Further scaling up is under way.

MC emulsification exploits the interfacial tension, the dominating force on a micrometer scale, as the driving force for droplet formation [29]. During the droplet formation, the distorted dispersed phase is spontaneously transformed into spherical droplets by interfacial tension. The dispersed phase is forced into a distorted (elongated) disk-like shape in the MC. This distorted disk-like shape is the essential point for spontaneous transformation since the disk-like shape has a higher interface area than a spherical shape, resulting in instability from the viewpoint of interface free energy. The dispersed phase with disk-like shape spontaneously transforms into spherical droplets. Therefore, the droplets are formed without shear by continuous phase flow, and the required energy input is very low compared with conventional emulsification techniques. The mechanism is similar to the breakup of cylindrical flow at the point where transformation is caused by interfacial tension [30]. Our previous study showed that the droplet diameter can be predicted from the MC structure based on the droplet formation mechanism [23]. The MC structure also affects the emulsion productivity [31]. The droplet formation behavior drastically changes above the critical flow velocity, and the critical flow velocity can be predicted by the critical capillary number [32]. The droplet formation is determined by the balance between the interfacial tension and viscous force.

In this study, W/O/W emulsions are prepared by a two-step emulsification employing MC emulsification as the second step. The mild action of MC emulsification, in which droplets are formed without shear by continuous phase flow, is expected to lead to a high entrapment yield of multiple emulsions. Although MC emulsification is the preferred first step, we used a homogenizer for the first step emulsification because of the limited production rate of MC emulsification. We prepared W/O/W emulsions with monodispersed oil droplets using MC emulsification by pressurizing the premixed W/O emulsions into the external water phase through the MC. A premixed polydispersed emulsion enables analyzing the behavior of the contained water droplets penetrating the MC in the second emulsification step. We then fluorometrically investigated the entrapment yield of the resulting W/O/W emulsion.

2. Materials and methods

2.1. Materials

Decane and ethyl oleate were purchased from Wako Pure Chemical Ind. (Osaka, Japan). Medium-chain triglyceride (MCT), with a fatty acid carbon number ranging from 8 to 10, was supplied by Taiyo Kagaku Co. Ltd. (Mie, Japan). Triolein (purity > 90%) was supplied by Nippon Lever B.V. (Tokyo, Japan). These were used as oil phases. Tris–HCl buffered (0.2 M, pH 9) Milli-Q water was used as internal and external water phases. Salt added in the internal water phase prevents the rapid coarsening of the W/O emulsion; salt added in the external phase balances the osmotic pressure. Tetraglycerin-condensed ricinoleic acid ester (CR-310, HLB < 1) is a suitable surfactant for preparing W/O emul-

sions. It was supplied by Sakamoto Yakuhin Kogyo Co. Ltd. (Osaka, Japan), and used to stabilize the premixed W/O emulsions. Pentaglycerin monolaurate (PGML; Sun soft A-121E; HLB = 12) was supplied by Taiyo Kagaku Co. Ltd., and was used to stabilize the O/W emulsion. Fluorescent dye (calcein) was purchased from Sigma Chemical Co. (St. Louis, MO, USA). Cobalt chloride ($CoCl_2$) was purchased from Kanto Chemical Co. Inc. (Tokyo, Japan). Calcein and $CoCl_2$ were used to determine the entrapment yields.

2.2. First-step emulsification

The first-step emulsification consists of preparing premixed polydisperse W/O emulsions. The premixed W/O emulsions were prepared using a homogenizer (Polytron PT-MR 3000; Kinematica AG, Littau, Switzerland). The homogenizer rotation speed and mixing time were controlled, as the premixed W/O emulsions have droplets with diameters from several to 100 μm. This wide range of droplet diameter distribution is useful for observing the variously sized internal water droplets penetrating through MCs.

2.3. MC emulsification

MC emulsification was used for the second step. The laboratory-scale apparatus for MC emulsification consists of a silicon MC plate, an MC module, and liquid chambers supplying continuous and dispersed phases [21]. Figure 1 depicts the experiment setup and schematic flow of the premixed W/O emulsion phase through the silicon MC. The emulsification was observed through the glass plate using a microscope with a differential interference contrast (DIC) mode and a fluorescent mode (DM IRM; Leica Microsystems AG, Wetzlar, Germany). In this study, a high-speed camera (Rabitt mini 2; Photoron, Tokyo, Japan), which can capture 600 frames/s, was also used to observe the emulsification. Figure 2 shows the silicon MC plate fabricated using photolithography and orientation-dependent etching processes [33]. The silicon MC plate measured 15 × 15 mm, and a 1-mm-diameter hole was produced at the center of the MC plate. Four 150-μm-high, 10-mm-long terrace lines were fabricated on the MC plate. In this study, 90 channels on each terrace line, 360 channels total, were fabricated and used. The MC module was initially filled with the external water phase. The W/O emulsion, which was pressurized by the head difference of the liquid chamber, entered the space between the silicon MC plate and the glass plate, and W/O/W droplets were formed from the MC. The prepared emulsion was recovered by an external water phase flow.

2.4. Measurement and analytical method

We determined the average diameters (D_a) (μm) and coefficients of variation (CV) (%) of the prepared emulsions from pictures of 100 droplets taken with the microscope

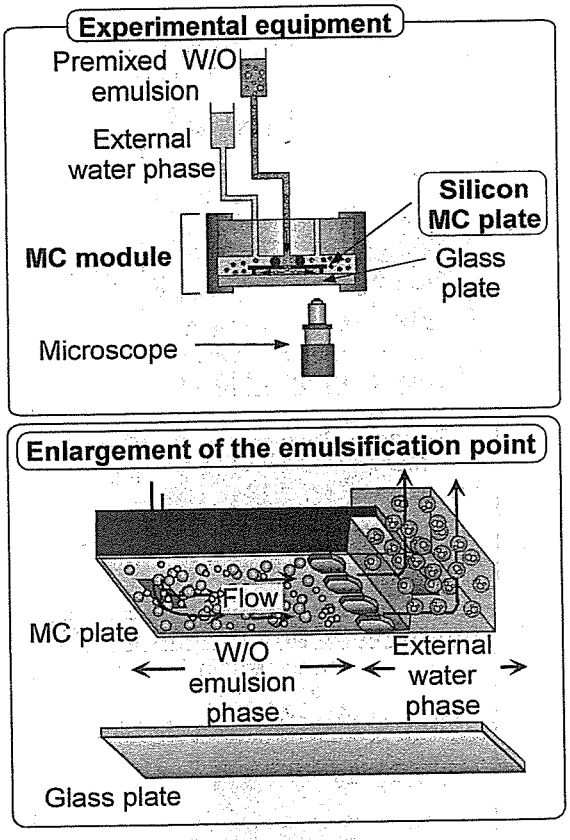

Fig. 1. Experimental setup and schematic flow of premixed W/O emulsion phase through the MC.

video system described above. The coefficient of variation is defined as

$$\mathrm{CV} = (\sigma/D_a) \times 100, \tag{1}$$

where σ is the standard deviation of the diameter (μm). Winroof (Mitani Corporation, Fukui, Japan) software was used to analyze the captured pictures. The viscosities of the organic solvents were measured with a Microviscometer (HAAKE, Karlsruhe, Germany). The viscosities of the oil phases containing 5% of the surfactant were measured.

Entrapment yield was determined fluorometrically by modifying the method used for determining the trapped volume of liposomes [34]. The calcein content in W/O/W emulsions was determined from the fluorescence intensity before and after cobalt(II) ions were added, which quench florescence of calcein by chelate formation. Fluorescence intensity was measured with a fluorescence spectrophotometer (FP-777; JASCO Co., Tokyo, Japan). The fluorescence intensity from 3 ml of W/O/W emulsions was measured before (F_{tot}) and after (F_{in}) addition of 30 μl of $CoCl_2$ (0.01 M). F_{tot} corresponds to the fluorescence from all materials composing the W/O/W emulsion. F_{in} corresponds to the fluorescence from the internal water phase plus the fluorescence from the W/O/W emulsion itself. The entrapment yield is calculated from the equation

$$\text{entrapment yield (\%)} = \frac{(F_{\mathrm{in}} - F_{\mathrm{wow}})}{(F_{\mathrm{tot}} - F_{\mathrm{wow}})} \times 100, \tag{2}$$

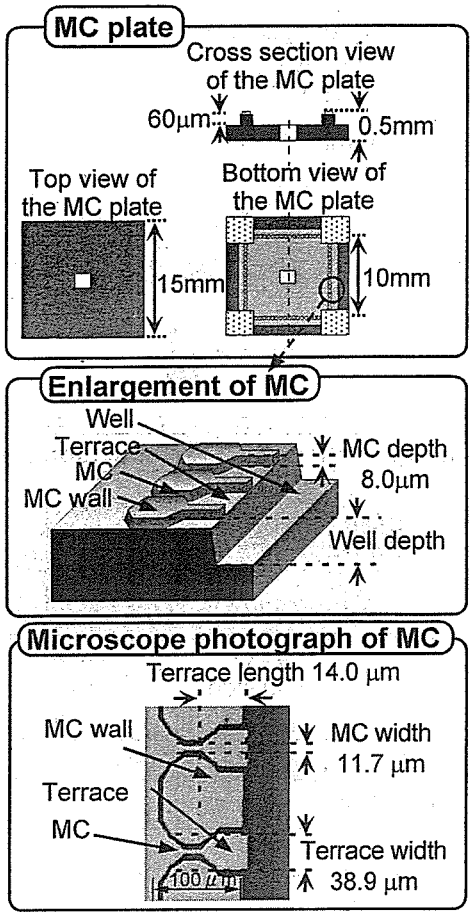

Fig. 2. Silicon MC plate.

where, F_{wow} represents the fluorescence intensity from the W/O/W emulsion itself, meaning the W/O/W emulsion without calcein, which was measured separately. The dilution from adding $CoCl_2$ solution can be neglected because of the small volume of the added solution. The entrapment yield calculated from Eq. (2) represents the ratio of the material amount entrapped in the internal water phase to the amount in the total recovered emulsion.

3. Results and discussion

3.1. Preparation of W/O/W emulsions using MC emulsification

First-step emulsification was performed with a homogenizer. Decane, ethyl oleate, MCT, and triolein were used as oil phases. Five percent of CR-310 was dissolved in each oil phase and used as the surfactant for W/O emulsion. Tris–HCl buffer was used for the internal water phases. The internal water phases were gently added to the oil phase by mixing with a homogenizer until the volume fraction of water phase reached 10%. The homogenizer rotation speed and mixing time were controlled as the premixed W/O emulsions have droplets with diameters ranging from 1 to 100 μm.

Table 1
Average diameters and coefficients of variation of the prepared W/O/W emulsions and the internal water droplets for four oil phases

Oil phase	Viscosity (mPa s)	$D_{a,\,W/O/W}$ (μm)	$CV_{W/O/W}$ (%)	$D_{a,\,W/O}$ (μm)	$CV_{W/O}$ (%)
Decane	1.3	32.6	5.5	21.0	26.8
Ethyl oleate	6.5	31.8	6.3	19.2	26.0
MCT	26	32.6	8.0	21.0	27.6
Triolein	69	35.7	19.0	17.9	29.6

CR-310 was used as a surfactant dissolved in oil phase. $D_{a,\,W/O/W}$ and $CV_{W/O/W}$ are the average diameter and the coefficient of variation for W/O/W emulsion. $D_{a,\,W/O}$ and $CV_{W/O}$ are the average diameter and the coefficient of variation for W/O emulsion.

Second-step emulsification was performed using MC emulsification, in which the premixed emulsions were pressurized into the external water phase. Tris–HCl buffer was used for the external water phase. The second-step MC emulsification was carried out at a W/O emulsion flow rate of 0.1 ml/h. In this case, no surfactant was added to the external water phase to avoid increasing its viscosity. Increased viscosity can lead to unsuccessful MC emulsification, especially for high-viscosity oil phases. Without surfactant in the external water phase, the prepared W/O/W emulsions were stable enough so that no coalescence was observed in the module. For long-time stability, a hydrophilic surfactant (high HLB) should be added after recovery of the W/O/W emulsion. Figure 3 shows the MC emulsification process observed through the microscope (DIC mode) using four oil phases. Figure 4 presents the prepared W/O/W emulsions observed through the microscope (DIC mode). Successful MC emulsification was observed for decane, ethyl oleate, and MCT, and monodispersed oil droplets containing small water droplets were prepared. MC emulsification was possible for triolein, but larger droplets were formed from some of the channels.

Figure 5 illustrates the droplet diameter distributions of the prepared W/O/W emulsions using four oil phases. D_a and CV of the W/O/W emulsions and the internal water droplets are shown in Table 1 for four oil phases. The internal water droplets, which were optically accessible (larger than 5 μm), were measured. Monodispersed oil droplets with CVs of 5 to 8% were prepared using decane, ethyl oleate, and MCT as oil phases. When the high-viscosity oil phases (MCT and triolein) were used, larger droplets formed and continuous outflow of the W/O emulsion phase occurred, resulting in a high CV of 19%.

In all cases, the droplet diameter distributions of the W/O/W emulsions were slightly wider than those in the previous study [29], where it was shown that the droplet diameter was affected by the viscosity ratio of the dispersed phase and the continuous phase [25]. If the dispersed phase is less viscous than the continuous phase, larger droplets are formed. The effective viscosity of a W/O emulsion, which corresponds to the dispersed phase in the second-step emulsification, is affected by the volume fraction of the internal water phase. During the MC emulsification, the volume

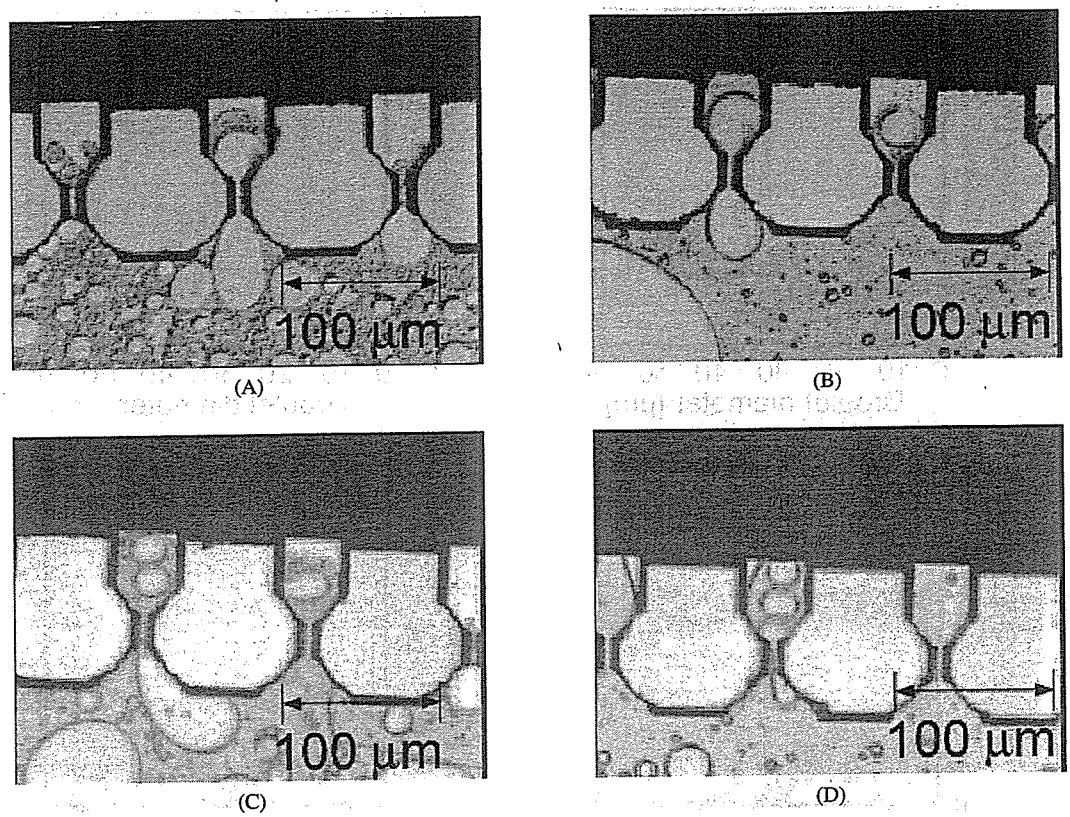

Fig. 3. Microscope photographs of MC emulsification process (DIC mode). Oil phases were decane (A), ethyl oleate (B), MCT (C), and triolein (D).

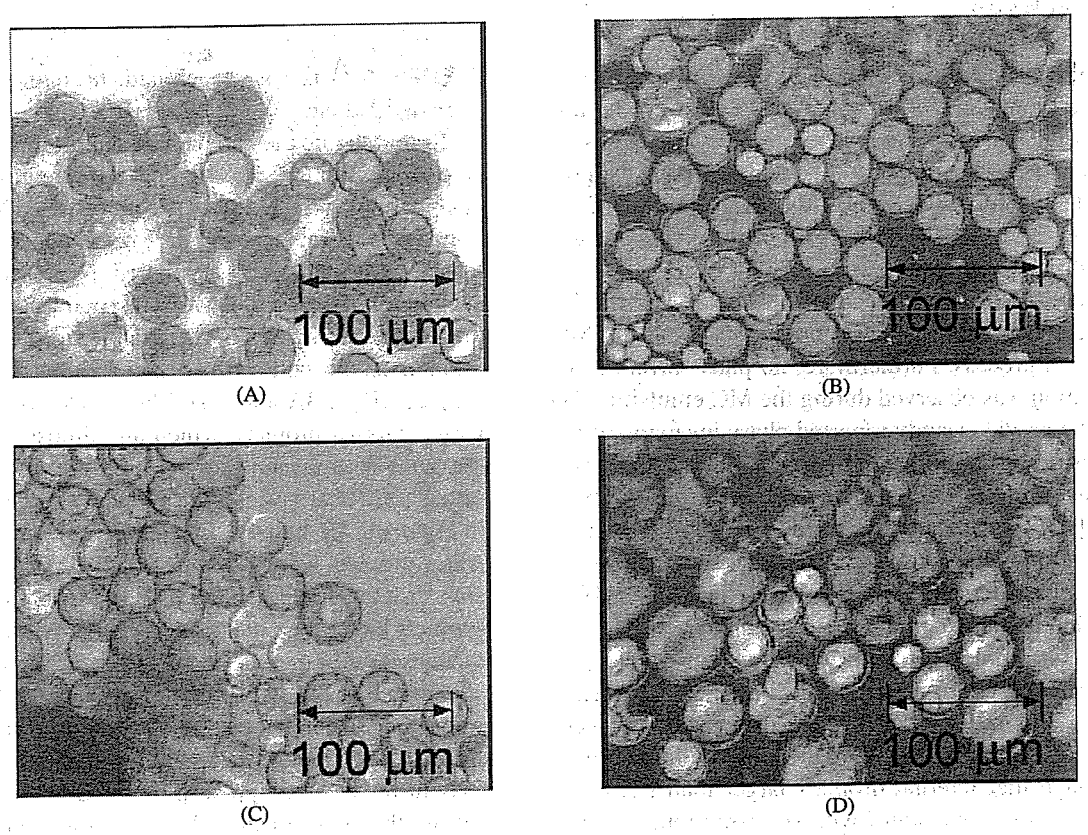

Fig. 4. Microscope photographs of prepared W/O/W emulsions (DIC mode). Oil phases were decane (A), ethyl oleate (B), MCT (C), and triolein (D).

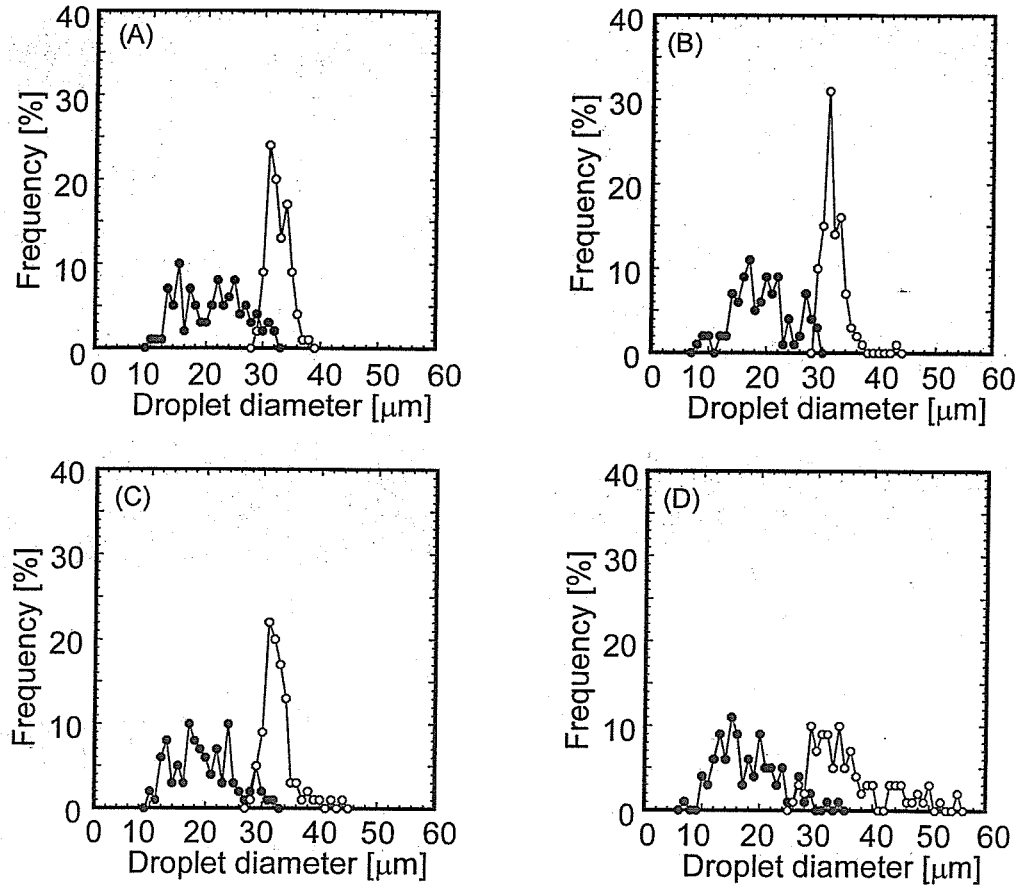

Fig. 5. Droplet diameter distributions of the prepared W/O/W emulsions (○) and internal water phases (●). Oil phases were decane (A), ethyl oleate (B), MCT (C), and triolein (D).

fractions of W/O emulsions penetrating the MC fluctuate because the premixed W/O emulsions do not have homogeneous structures on a microscopic scale. This leads to fluctuation in the viscosity of W/O emulsions and in the prepared droplet diameters. Consequently, the resulting W/O/W emulsions have larger CVs than those of the emulsions described in the previous study.

It is important to point out that no leakage of the internal water phase was observed optically during the MC emulsification process. Furthermore, no phase inversion or demulsification was observed during the MC emulsification process. The previous study reported phase inversion of the O/W emulsion produced using hydrophobic MC [35]. Hydrophilic membranes were also applied to disrupt the W/O emulsion [36]. Whether the dispersed phase is disrupted or penetrated may depend on the stabilization effect of the surfactant molecules added in the oil phases. The surfactant used in this study (CR-310) is known to effectively stabilize water droplets in oil and therefore could have prevented disruption of the thin oil film between the internal water phase and external water phase during MC emulsification. Interestingly, the thin oil film between the phases is strong enough that internal droplets larger than MCs also penetrated through the channel without disruption, as shown in Fig. 3. Internal water droplets larger than the resulting W/O/W droplets also penetrated through the channel and were divided into several droplets.

To investigate the behavior of the internal water droplets penetrating the MC, we studied the changes of the droplet diameters of the internal water phase after MC emulsification. We also investigated the size changes of the discrete internal water droplets and plotted the results in Fig. 6. For decane, ethyl oleate, and MCT, internal water droplets larger than the resulting W/O/W emulsion droplets were divided into almost the same size as the resulting W/O/W emulsion droplets (Figs. 3A and 3B). These W/O/W emulsions have larger internal droplets, which are almost the same size as the W/O/W emulsion droplets, and oil phases are like thin oil layers. These vesicle-like W/O/W emulsions were found in Figs. 4A, 4B, and 4C. In contrast, several smaller internal water droplets were entrapped into a single W/O/W emulsion droplet (Fig. 4). For MCT and triolein, internal water droplets larger than the resulting W/O/W emulsion droplets were sheared at the MC and divided into smaller droplets, as shown in Figs. 3C and 3D. The larger internal water droplets might have been sheared at the MC by the high-viscosity flow of MCT and triolein, and the sheared smaller droplets may have been entrapped in the W/O/W emulsion droplets during the detachment of W/O/W emulsion droplets. In all cases, the strong stabilizing effect of CR-310 and the mild

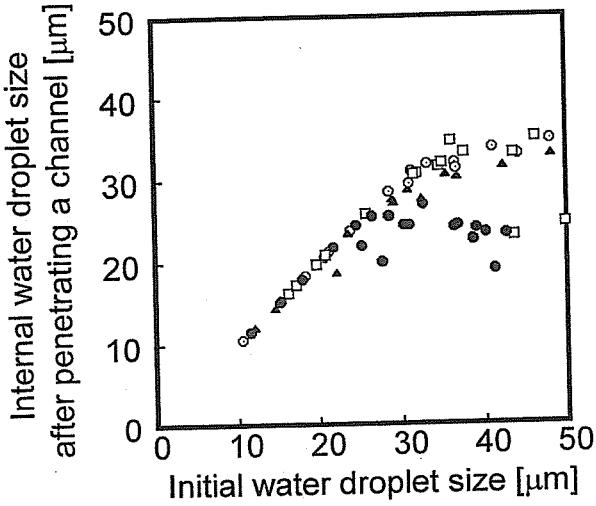

Fig. 6. Changes of the droplet diameter of internal water phase after MC emulsification. Oil phases were decane (○), ethyl oleate (▲), MCT (□), and triolein (●).

Table 2
Fluorescence intensities of calcein entrapped in W/O/W emulsion

No.	Sample	Fluorescence intensity (arbitrary units)
1	W/O/W emulsion containing calcein (F_{tot})	3650
2	W/O/W emulsion containing calcein + $CoCl_2$ (F_{in})	3393
3	W/O/W emulsion without calcein (F_{WOW})	735
4	Calcein in Tris–HCl buffer	2507
5	Calcein in Tris–HCl buffer + $CoCl_2$	1.58

The voltage applied to the photomultiplier was high-mode for samples 1, 2, and 3, and low-mode for samples 4 and 5.

droplet formation action of MC emulsification resulted in effective entrapment of the internal water phase without disruption.

3.2. Entrapment yield in W/O/W emulsion

We studied the entrapment yield fluorometrically using calcein solution. Tris–HCl buffer containing 4×10^{-4} M calcein was used as the internal water phase. MCT with 5% CR-310 was used as the oil phase. Tris–HCl buffer containing 1% PGML was used as the external water phase. The first-step emulsification was performed using a homogenizer at 5000 rpm for 3 min. The internal water phases were gently added to the oil phases by mixing with a homogenizer until the volume fraction of the water phase reached 10%. The second-step MC emulsification was conducted at a 0.1 ml/h W/O emulsion flow rate for 1 h. The prepared W/O/W emulsion was recovered by 100 ml of external water phase. The resulting oil-phase content in the external water phase was approximately 0.1%. The final calcein concentration was calculated to be approximately 4×10^{-8} M.

Figure 7 presents the prepared W/O/W emulsion observed using a microscope in DIC mode (Fig. 7A) and fluorescent mode (Fig. 7B). The fluorescent image shows

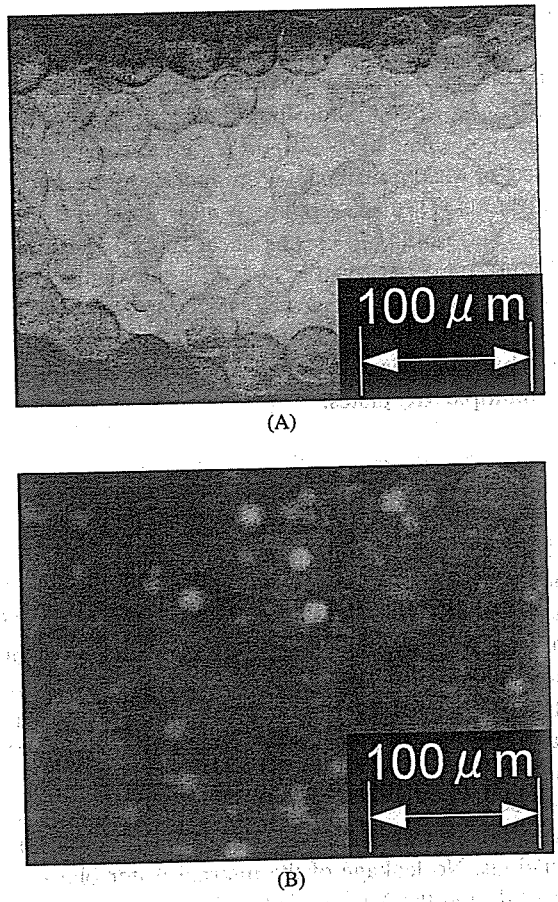

Fig. 7. Microscope photographs of the prepared W/O/W emulsion observed in DIC mode (A) and fluorescence mode (B).

the discrete internal water droplets inside the W/O/W emulsions. No fluorescence was observed outside the W/O/W emulsions, indicating a high entrapment yield. Table 2 lists the fluorescence intensities of calcein entrapped in W/O/W emulsions. The entrapment yield calculated by Eq. (2) was 91%. The mild action of droplet formation during MC emulsification led to high entrapment yields. The fluorescence from W/O/W emulsion itself is not negligible (Table 2, No. 3) but is corrected by Eq. (2). We conducted a control experiment in order to confirm the quenching ability of cobalt ions. The fluorescence of 3 ml of the 4×10^{-6} M calcein solution was measured before (Table 2, No. 4) and after (Table 2, No. 5) the addition of 30 μl of $CoCl_2$ (0.01 M). The control experiment revealed that the cobalt ion is a very efficient quencher of calcein fluorescence. The above results demonstrate that MC emulsification enables preparing W/O/W multiple emulsions with high entrapment yields because of its mild action during droplet formation.

We think that other methods, such as membrane emulsification and shear rupturing, also provide high entrapment yields. In particular, the shear-rupturing method provides high entrapment yields close to 98% [20]. Compared to the membrane emulsification method, MC emulsification has superior monodispersity. Using membrane emulsification, it is difficult to produce emulsions with a CV of less than 10%.

MC emulsification is more useful than the shear-rupturing method for producing emulsions with low viscosity oil and water phases. The shear rupturing method is applied only for highly viscous continuous phase because droplet formation is based on shear stress [20]. In regard to the droplet diameter range, MC emulsification produces larger emulsions (up to 100 μm [37]) than membrane emulsification (submicrometers to 60 μm [16]) and the shear-rupturing method (1 to 20 μm [20]). A disadvantage of MC emulsification is its low production rate. However, we believe MC emulsification can be scaled up by a factor of 10^3 to 10^4 compared with this study by using a larger MC plate, straight-through MC [24], and multiple MC plates.

4. Summary

MC emulsification was applied to prepare W/O/W emulsions using four oil phases. Successful MC emulsification was observed for decane, ethyl oleate, and MCT, and monodispersed oil droplets containing small water droplets were prepared. MC emulsification was possible for triolein, but larger droplets were formed from some of the channels. In all cases, the droplet diameter distributions of the W/O/W emulsion were slightly wider than those in the previous study because the viscosity of the premixed W/O emulsions fluctuated due to the non-homogeneous structure of the W/O emulsions. No leakage of the internal water phase was observed during the MC emulsification process. Furthermore, internal droplets larger than the MC also penetrated through the channel without disrupting the thin oil film. For decane, ethyl oleate, and MCT, internal water droplets larger than the resulting W/O/W emulsion droplets were divided into almost the same size as the resulting W/O/W emulsion droplets. For MCT and triolein, internal water droplets larger than the resulting W/O/W emulsion droplets were sheared at the MC and divided into smaller droplets. The entrapment yield in a W/O/W emulsion was measured fluorometrically and determined to be 91%. MC emulsification has the advantage of a high entrapment yield, resulting from mild action during droplet formation.

Acknowledgments

We thank Dr. K. Nagayama (Kochi National College of Technology) for his advice on our experimental system. We also thank Taiyo Kagaku Co. Ltd. for providing MCT and Sakamoto Yakuhin Kogyo Co. Ltd. for providing glycerin condensed ricinoleic acid esters and polyglycerin fatty acid esters. This work was supported by MAFF, Program for Nanotechnology Project, and the Program for Promotion of Fundamental Studies in Health Sciences of the Organization for Pharmaceutical Safety and Research of Japan.

References

[1] W. Seifriz, J. Phys. Chem. 29 (1925) 738.
[2] P. Sherman (Ed.), Emulsion Science, Academic Press, New York, 1968, p. 206.
[3] S. Matsumoto, J. Colloid Interface Sci. 94 (1983) 362.
[4] P. Becher, J. Soc. Cosmetic Chem. 9 (1958) 141.
[5] S. Matsumoto, Y. Kita, D. Yonezawa, J. Colloid Interface Sci. 57 (1976) 353.
[6] H. Okochi, M. Nakano, Chem. Pharm. Bull. 44 (1996) 180.
[7] J.A. Omotosho, A.T. Florence, T.L. Whateley, Int. J. Pharm. 61 (1990) 51.
[8] A.T. Florence, D. Whitehill, J. Pharm. 11 (1982) 277.
[9] M.F. Ficheux, L. Bonakdar, F. Leal-Calderon, J. Bibette, Langmuir 14 (1998) 2702.
[10] N. Garti, Colloids Surf. A 123–124 (1997) 233.
[11] W. Hou, K.D. Papadopoulos, Chem. Eng. Sci. 51 (1996) 5043.
[12] A.T. Florence, D. Whitehill, J. Colloid Interface Sci. 79 (1981) 243.
[13] J. Bibette, D. Roux, F. Nallet, Phys. Rev. Lett. 65 (1990) 2470.
[14] J. Bibette, J. Colloid Interface Sci. 147 (1991) 474.
[15] T. Nakashima, M. Shimizu, M. Kukizaki, Key Eng. Mater. 61/62 (1991) 513.
[16] T. Nakashima, M. Shimizu, M. Kukizaki, Adv. Drug Deliv. Rev. 45 (2000) 47.
[17] Y. Mine, M. Shimizu, T. Nakashima, Colloids Surf. B 6 (1996) 261.
[18] S. Higashi, M. Shimizu, T. Nakashima, K. Iwata, F. Uchiyama, S. Tateno, S. Tamura, T. Setoguchi, Cancer 75 (1995) 1245.
[19] T.G. Mason, J. Bibette, Langmuir 13 (1997) 4600.
[20] C. Goubault, K. Pays, D. Olea, P. Gorria, J. Bibette, V. Schmitt, F. Leal-Calderon, Langmuir 17 (2001) 5184.
[21] T. Kawakatsu, Y. Kikuchi, M. Nakajima, J. Am. Oil Chem. Soc. 74 (1997) 317.
[22] T. Kawakatsu, G. Trägårdh, Y. Kikuchi, M. Nakajima, H. Komori, T. Yonemoto, J. Surfact. Deterg. 3 (2000) 295.
[23] S. Sugiura, M. Nakajima, M. Seki, Langmuir 18 (2002) 3854.
[24] I. Kobayashi, M. Nakajima, K. Chun, Y. Kikuchi, H. Fujita, AIChE J. 48 (2002) 1639.
[25] T. Kawakatsu, G. Trägårdh, C. Trägårdh, M. Nakajima, N. Oda, T. Yonemoto, Colloids Surf. A 179 (2001) 29.
[26] S. Sugiura, M. Nakajima, H. Ushijima, K. Yamamoto, M. Seki, J. Chem. Eng. Jpn. 34 (2001) 757.
[27] S. Sugiura, M. Nakajima, J. Tong, H. Nabetani, M. Seki, J. Colloid Interface Sci. 227 (2000) 95.
[28] S. Sugiura, M. Nakajima, H. Itou, M. Seki, Macromol. Rapid Commun. 22 (2001) 773.
[29] S. Sugiura, M. Nakajima, S. Iwamoto, M. Seki, Langmuir 17 (2001) 5562.
[30] J. Eggers, Rev. Mod. Phys. 69 (1997) 865.
[31] S. Sugiura, M. Nakajima, M. Seki, Langmuir 18 (2002) 5708.
[32] S. Sugiura, M. Nakajima, N. Kumazawa, S. Iwamoto, M. Seki, J. Phys. Chem. B 106 (2002) 9405.
[33] Y. Kikuchi, K. Sato, H. Ohki, T. Kaneko, Microvascular Res. 44 (1992) 226.
[34] N. Oku, D.A. Kendall, R.C. Macdonald, Biochim. Biophys. Acta 691 (1982) 332.
[35] T. Kawakatsu, R.M. Boom, H. Nabetani, Y. Kikuchi, M. Nakajima, AIChE J. 45 (1999) 967.
[36] J.T.F. Keurentjes, G.I. Doonbusch, K.V. Riet, Sep. Sci. Technol. 26 (1991) 409.
[37] S. Sugiura, M. Nakajima, N. Kumazawa, M. Seki, J. Am. Oil Chem. Soc. 79 (2002) 515.

Primary Mediastinal Lymphoma

Characteristic Features of the Various Histological Subtypes on CT

Ukihide Tateishi, MD, PhD, Nestor L. Müller, MD, PhD,† Takeshi Johkoh, MD, PhD,‡ Yasushi Onishi, MD,§ Yasuaki Arai, MD, PhD,* Mitsuo Satake, MD,* Yoshihiro Matsuno, MD, PhD,‖ and Kensei Tobinai, MD, PhD§*

Objective: To assess the characteristic features of the primary mediastinal lymphoma (PML) on CT and to test the relationship between CT findings and the likelihood of the 3 most common subtypes (Hodgkin lymphoma [HL], mediastinal diffuse large B-cell lymphoma [Med-DLBCL], and precursor T-cell lymphoblastic lymphoma [T-LBL]).

Methods: Sixty-six consecutive patients with pathologically proven PML including 29 patients with HL, 21 with Med-DLBCL, and 16 with T-LBL underwent CT prior to therapy. CT scans were independently reviewed by 2 radiologists who were blinded to the pathologic diagnosis for the following considerations: pattern of involvement (i.e., morphologic features, mass size, and contrast enhancement pattern), and ancillary findings at other sites including neck, abdomen, and pelvis. Interobserver agreement was measured by Kappa statistics, and independent predictors were calculated using multiple logistic regression analysis for determining the likelihood of the subtypes based on CT.

Results: Characteristic features of HL included irregular contour of the anterior mediastinal mass (20 of 29, 69%) and high prevalence of associated mediastinal lymphadenopathy (28 of 29, 97%). Characteristic features of Med-DLBCL included regular contour (14 of 21, 67%) and absence of cervical and abdominal lymphadenopathy (0 of 21). Characteristic features of T-LBL included regular contour (12 of 16, 75%) and high prevalence of cervical (9 of 16, 56%) and abdominal (6 of 16, 38%) lymphadenopathy and splenomegaly (11 of 16, 69%). CT findings independently associated with increased likelihood of HL were surface lobulation ($P < 0.01$), the absence of vascular involvement ($P < 0.01$), or pleural effusion ($P < 0.05$). The presence of vascular involvement was associated with increased likelihood of Med-DLBCL ($P < 0.001$). Furthermore, CT findings including the presence of cervical lymph nodes or inguinal lymph nodes ($P < 0.001$), the presence of pericardial effusion ($P < 0.05$), and the absence of surface lobulation ($P < 0.05$) were significantly associated with the likelihood of T-LBL.

Conclusion: The various histologic subtypes of PML have characteristic manifestations in the neck, chest, and abdomen, which allow their distinction on CT.

Key Words: malignant lymphoma, mediastinal tumor, computed tomography

(*J Comput Assist Tomogr* 2004;28:782–789)

Malignant lymphoma that involves mainly or exclusively the mediastinum at initial presentation (primary mediastinal lymphoma: PML) is a relatively common condition seen in patients of all ages.[1–4] Most cases are due to 1 of 3 histologic subtypes: Hodgkin lymphoma (HL), mediastinal diffuse large B-cell lymphoma (Med-DLBCL), and precursor T-cell lymphoblastic lymphoma (T-LBL). Distinction of the specific histologic subtype is important as it influences treatment and prognosis.[5–12] Because the specific diagnosis should be confirmed by immunohistochemical analysis and hence requires large tissue samples, it is not always easy to make a confident diagnosis on biopsy specimens.[7–10]

There is a sizable body of literature examining the distribution of nodes or masses in lymphoma.[13–27] However, there is limited information on the characteristic manifestations of the various subtypes of PML and the potential value of CT in the differential diagnosis. CT has been increasingly used for the evaluation of patients with suspected or proven lymphoma. It allows for accurate staging of the disease and follow-up of the therapeutic response.[15–23] The purpose of the present study was to assess the characteristic features of the various histologic subtypes of PML and the diagnostic accuracy of CT evaluation for a specific histologic subtype.

MATERIALS AND METHODS

Patients

Sixty-six cases of PML were registered in the radiologic files of our institute. Clinical details and follow-up information including the presence or absence of recurrence were reviewed retrospectively by a hematologic oncologist who was one of the authors. Our institutional review board does not require its approval or patient informed consent for this type of review. The study included 45 men (mean age 38.4 years, range 16 to 84 years) and 21 women (mean age 34.1 years, range 13 to 63 years). All patients underwent uniform staging that included a physical examination, blood cell counts, routine blood

From the *Division of Diagnostic Radiology, National Cancer Center Hospital, Tokyo, Japan; †Division of Hematologic Oncology, National Cancer Center Hospital, Tokyo, Japan; ‖Division of Pathology, National Cancer Center Hospital, Tokyo, Japan; †Department of Radiology, University of British Colombia and Vancouver Hospital and Health Sciences Centre, Canada; and ‡Department of Medical Physics, Osaka University Graduate School of Medicine, Osaka, Japan.

Reprints: Ukihide Tateishi, MD, PhD, Division of Diagnostic Radiology, National Cancer Center Hospital, Tsukiji, Chuo-Ku, 104-0045, Tokyo, Japan (E-mail: utateish@ncc.go.jp).

chemistries, and bone marrow aspiration. Clinical features, International Prognostic Index (IPI) scores,[28] and clinical stages were recorded.

Histopathologic confirmation of definite diagnosis in all patients was obtained by core needle or excisional biopsy. Biopsy sites included the anterior mediastinal mass in 33 patients, cervical lymph node in 25, and both in 8. Fifty-four patients (82%) were confirmed by the initial biopsy alone and the other 12 patients (18%) underwent subsequent biopsy because of insufficient initial sample.

Immunohistochemical studies to determine histologic subtype were performed in all biopsy specimens. According to a recent classification system[29] devised by the World Health Organization (WHO), 29 patients had classic HL, 21 had Med-DLBCL, and 16 had T-LBL. The presence or absence of nodal involvement in each suspected lesion was determined at biopsy in 36 sites and the remaining with a combination of imaging findings and clinical follow-up. Extranodal involvement in the abdomen confirmed by endoscopic, needle, or excisional biopsy included stomach (n = 1), kidney (n = 1), and spleen (n = 1).

The histopathologic findings were reviewed by an experienced pathologist who was one of the authors. Chart, review of histologic specimens, and patient file reviews were

TABLE 1. CT Findings in Patients With PML and the Other Common Nonlymphomatous Diseases

Disease	PML	Thymoma	Thymic cancer	GCT	SCLC
No. of patients	66	19	26	13	12
Male/female	45/21	8/11	18/8	13/0	9/3
Age (mean ± SD) (y)	37.0 ± 14.9	55.6 ± 12.2	58.4 ± 11.6	26.5 ± 5.4	64.5 ± 8.3
Age range (y)	13–84	29–74	24–74	18–38	51–78
Tumor margins*					
Well-defined margins	39 (59)	18 (95)	22 (85)	1 (8)	0
Ill-defined margins	27 (41)	1 (5)	4 (15)	12 (92)	12 (100)
Size of main mass (mean ± SD) [cm]	8.9 ± 3.0	5.2 ± 1.8	7.2 ± 2.4	11.6 ± 2.2	5.6 ± 1.6
Presence of surface lobulation	31 (47)	7 (37)	19 (73)	0	12 (100)
Presence of vascular encasement	21 (32)	1 (5)	20 (77)	7 (54)	2 (17)
Presence of chest wall invasion	10 (15)	0	13 (50)	3 (23)	0
Presence of cutaneous involvement	3 (5)	0	0	0	0
Presence of lung invasion†	11 (17)	0	0	0	NA
Presence of nodal involvement					
Cervical lymph node (superficial)†	10 (15)	0	0	0	0
Cervical lymph node (deep)§	18 (27)	0	0	0	0
Submandibular lymph node	1 (2)	0	0	0	0
Submental lymph node	2 (3)	0	0	0	0
Parotid lymph node	2 (3)	0	0	0	0
Supraclavicular lymph node	11 (17)	0	0	0	10 (83)
Mediastinal lymph node§	50 (76)	0	12 (46)	1 (8)	12 (100)
Hilar lymph node†	12 (15)	0	2 (8)	2 (15)	12 (100)
Axillary lymph node§	12 (15)	0	0	0	0
Celiac lymph node	4 (6)	0	0	0	0
Paraaortic lymph node§	12 (15)	0	0	0	0
Mesenteric lymph node	2 (3)	0	0	0	0
Iliac lymph node	1 (2)	0	0	0	0
Inguinal lymph node*	5 (8)	0	0	0	0
Presence of pleural effusion	26 (39)	2 (10)	8 (31)	5 (38)	5 (42)
Presence of pericardial effusion*	24 (36)	0	4 (15)	3 (23)	3 (25)
Hepatomegaly	2 (3)	0	0	0	0
Splenomegaly§	13 (20)	0	0	0	0
Presence of metastasis					
Lung metastasis§	0	0	5 (19)	7 (54)	3 (25)
Liver metastasis§	0	0	1 (4)	1 (8)	5 (42)
Splenic metastasis	1 (2)	0	0	1 (8)	0
Adrenal metastasis	0	0	0	0	1 (8)
Presence of pleural dissemination	13 (20)	2 (10)	6 (23)	2 (15)	2 (17)

Data in parentheses are percentages.
*$P < 0.05$, †$P < 0.01$, §$P < 0.0001$.
PML, Primary mediastinal lymphoma; GCT, germ cell tumor; SCLC, small cell lung cancer; NA, not applicable.

conducted independently of the CT analysis. All patients with PML underwent treatment, which included chemotherapy and radiotherapy for HL, chemotherapy and/or radiotherapy for Med-DLBCL, and chemotherapy and radiotherapy for T-LBL. Follow-up documentation was reviewed for any evidence of misdiagnosis at any repeat imaging examinations, biopsies, laboratory tests, or on the basis of ongoing symptoms and signs. At the time of this review, there has been no case of initial misdiagnosis.

To determine whether or not CT findings can accurately differentiate PML from the other common nonlymphomatous diseases, a total of 70 patients including thymoma (n = 19), thymic cancer (n = 26), germ cell tumor (n = 13), and small cell lung cancer (n = 12) were also enrolled in this study (Table 1). Selective criteria of these cases were 1) main anterior mediastinal mass identified on CT at presentation, 2) definite diagnosis confirmed by the pathologic observation of main mass, and 3) CT examination performed prior to therapy. These cases were selected from the radiologic files of our institute, and clinical details and follow-up information were also reviewed retrospectively by a radiologist who was one of the authors.

Imaging Studies

CT was performed on a 4-row multidetector scanner (Aquilion V-detector, Toshiba Medical Systems, Tokyo, Japan). The images were obtained at 240–260 mAs, 120 kV, 7-mm collimation sections overlapped in 3.5-mm intervals from the level of the orbit to the proximal femur, and a pitch of 10.5. All patients received 150 mL of nonionic intravenously administered contrast material at 3.0 mL/s with a power injector (Autoenhance A-250; Nemoto-kyorindo, Tokyo, Japan) after a 60-second delay. All patients also received 200–300 mL of sterile water orally prior to CT examination.

Image Analysis

Two experienced radiologists who had knowledge of the diagnosis of primary mediastinal lymphoma but were blinded to histologic subtypes and any clinical information other than patient age and sex independently reviewed the CT images on hard copies. The 2 readers analyzed the images for tumor size, tumor margins (well defined or ill defined), and presence of surface lobulation. The presence of a single mass or confluent lymphadenopathy in the anterior mediastinum was analyzed as representing the primary tumor mass and the measurement based on the short axis diameter. The contrast enhancement of the primary lesions was compared with that of normal muscle. The tumor was considered homogeneous if it enhanced to the same degree throughout. The patterns of local invasion were recorded: encasement of vascular structures, chest wall invasion, cutaneous involvement, and lung invasion. Vascular encasement was considered present when there was circumferential narrowing or complete obstruction of the superior vena cava or brachiocephalic vein by tumor. The presence or absence of lymphadenopathy, pleural effusion, pericardial effusion, and other organ involvement were also evaluated. Nodes were considered enlarged when their short axis diameter was greater than 10 mm. Hepatomegaly and splenomegaly were considered present when the liver and spleen were greater than 13 cm and 12 cm in longitudinal diameter at the midclavicular line, respectively.[29]

Statistical Analysis

Kruskal-Wallis test was used to compare the clinical variables and all CT findings in the 3 histologic subtypes of PML and the other common nonlymphomatous disorders. Student t test was used to compare mean tumor size of the mediastinal mass. The interobserver variation in the interpretation of all CT findings was analyzed using Kappa statistics. The interobserver agreement was classified as follows: poor, k = 0–0.20; fair, k = 0.21–0.40; moderate, k = 0.41–0.60; good, k = 0.61–0.80; and excellent, k = 0.81–1.00. The relationship between CT findings and the likelihood of the histologic subtypes was tested for independent predictors using multiple logistic regression analysis, which determined the odds ratio after adjusting for the other variables examined. All P values less than 0.05 were considered to indicate a statistically significant difference.

RESULTS

Statistically significant CT findings which have possibility of discriminating PML from the other common nonlymphomatous diseases were tumor margins, the presence of lung invasion, involvement of various lymph nodes including cervical (superficial and deep), mediastinal, hilar, axillary, paraaortic, inguinal lymph nodes, the presence of pericardial effusion, splenomegaly, the presence of lung metastasis, and liver metastasis. Patient demographics are listed in Table 2. Patients with Med-DLBCL were slightly older (mean age ± SD: 46.4 ± 18.0) than those with HL (34.6 ± 10.7) or T-LBL (30.6 ± 12.4) ($P < 0.01$). No other significant difference was seen in patient demographics between the 3 subtypes of PML.

TABLE 2. Demographic and Clinical Data in Patients With PML

Disease	HL	Med-DLBCL	T-LBL
No. of patients	29 (44)	21 (32)	16 (24)
Age (mean ± SD) (y)	34.6 ± 10.7	46.4 ± 18.0	30.6 ± 12.4*
Age range (y)	19–57	23–84	13–64
Gender			
Male	17 (59)	15 (71)	13 (81)
Female	12 (41)	6 (29)	3 (19)
IPI score			
Low	23 (79)	12 (57)	6 (38)
Low–intermediate	5 (17)	2 (10)	8 (50)
Intermediate–high	0	5 (24)	1 (6)
High	1 (3)	2 (10)	1 (6)
Clinical stage			
I	7 (24)	11 (52)	2 (13)
II	15 (52)	3 (14)	2 (13)
III	4 (14)	1 (5)	3 (19)
IV	3 (10)	6 (29)	9 (56)

Data in parentheses are percentages. Significant difference is found in the mean age between Med-DLBCL and T-LBL (*$P < 0.01$).

HL, Hodgkin lymphoma; Med-DLBCL, mediastinal diffuse large B-cell lymphoma; T-LBL, T-cell lymphoblastic lymphoma; IPI, International Prognostic Index.

Enlargement of cervical lymph nodes was seen more commonly in T-LBL (10 of 16 patients, 63%) than in HL (9 of 29 patients, 31%) ($P < 0.05$) and was not present in any of the patients with Med-DLBCL (Fig. 1). Of the cervical nodes, deep cervical nodes were affected more frequently in HL (31% [9 of 29 patients]) or T-LBL (56% [9 of 16 patients]) than those in Med-DLBCL (no patients). Superficial nodes were also involved more often in T-LBL (44% [7 of 16 patients]) than in HL (10% [3 of 29 patients], $P < 0.05$). Involvement of supraclavicular lymph nodes was seen more frequently in T-LBL (50% [8 of 16 patients]) compared with that in HL (10% [3 of 29 patients], $P < 0.01$). Submandibular, submental, and parotid lymph nodes were involved only in T-LBL (19% [3 of 16 patients]).

No significant difference was found in the size and margin of the primary lesion between the three histologic subtypes (Table 3). Surface lobulation (Fig. 2) was more common in HL (69% [20 of 29 patients]) than in both Med-DLBCL (33% [7 of 21 patients]) and T-LBL (25% [4 of 16 patients]) ($P < 0.01$, Table 3). The prevalence of vascular involvement including encasement of superior vena cava and left brachiocephalic vein in Med-DLBCL (62% [13 of 21 patients], $P < 0.0001$) and T-LBL (38% [6 of 16 patients],

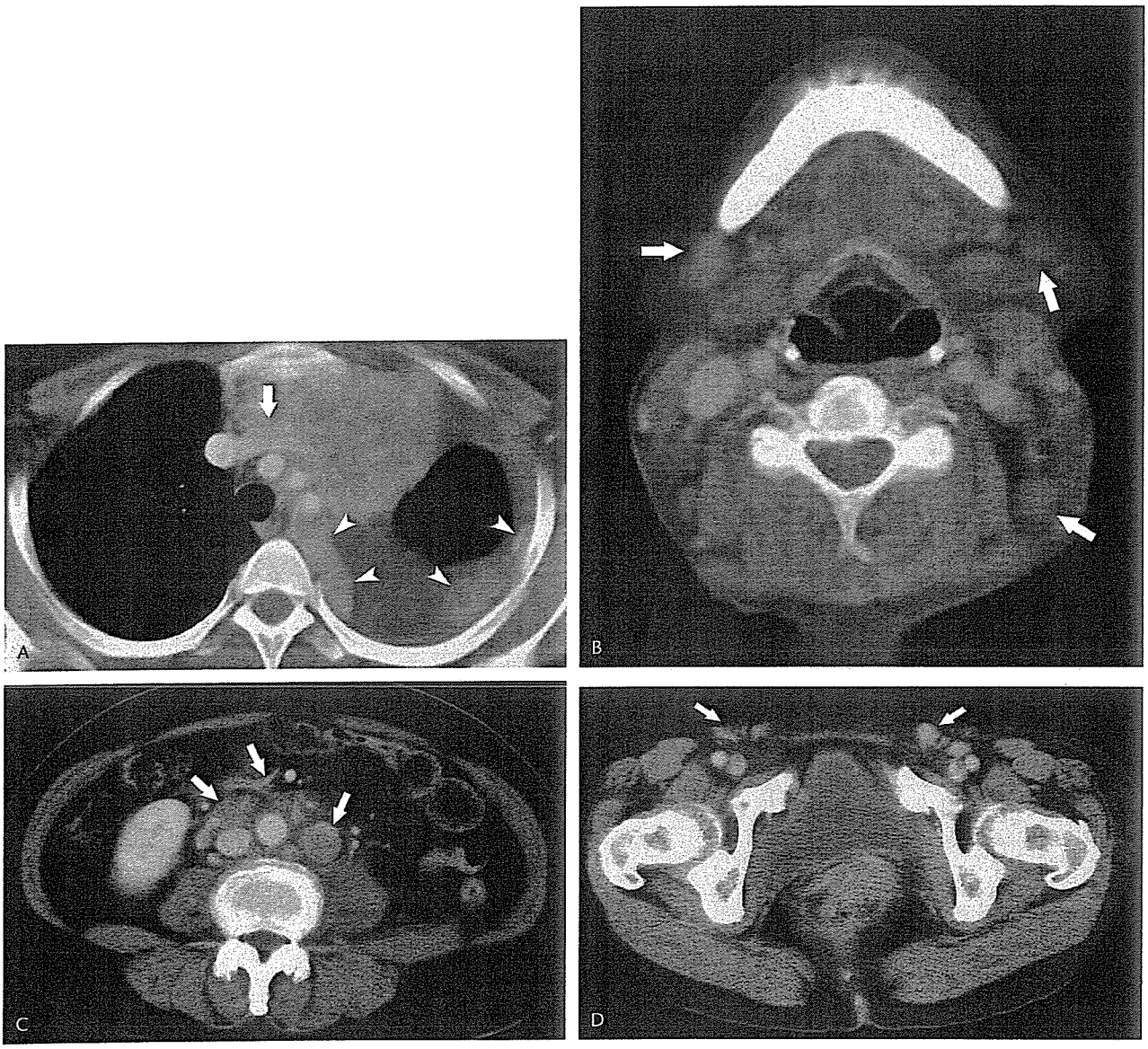

FIGURE 1. Thirty-two-year-old man with T-cell lymphoblastic lymphoma (T-LBL). A, Image obtained at the level of the great vessels shows a large anterior mediastinal mass with encasement and stenosis of the left brachiocephalic vein (arrow). Also noted are left pleural effusion and soft-tissue masses (arrowheads) in the left pleura suggestive of pleural dissemination. B, Image at the level of the upper neck demonstrates several enlarged of cervical nodes (arrows). C, Image at the level of the lower pole of the right kidney shows multiple enlarged paraaortic and mesenteric nodes. D, Image at the level of the inguinal region shows enlarged inguinal lymph nodes (arrows).